

# Weakly But Deeply Supervised Occlusion-Reasoned Parametric Layouts

Buyu Liu<sup>1</sup> Bingbing Zhuang<sup>1</sup> Manmohan Chandraker<sup>1,2</sup>  
<sup>1</sup>NEC Laboratories America <sup>2</sup>UC San Diego

## Abstract

We propose an end-to-end network that takes a single perspective RGB image of a complex road scene as input, to produce occlusion-reasoned layouts in perspective space as well as a top-view parametric space. In contrast to prior works that require dense supervision such as semantic labels in perspective view, the only human annotations required by our method are for parametric attributes that are cheaper and less ambiguous to obtain. To solve this challenging task, our design is comprised of modules that incorporate inductive biases to learn occlusion-reasoning, geometric transformation and semantic abstraction, where each module may be supervised by appropriately transforming the parametric annotations. We demonstrate how our design choices and proposed deep supervision help achieve accurate predictions and meaningful representations. We validate our approach on two public datasets, KITTI and NuScenes, to achieve state-of-the-art results with considerably lower human supervision.

## 1. Introduction

Understanding road layout from images is essential for real-world applications such as autonomous driving or path planning [11, 3, 6, 25], where besides the usual perspective space outputs, top-view representations of geometry and semantics have been popular. Non-parametric representations such as pixel-level semantics [25] generally require labor-intensive and potentially ambiguous supervision in the top-view, for example, when dealing with occluded regions. On the other hand, parametric representations for top-view layout are desirable for their interpretability, which is beneficial for higher-level reasoning and decision-making in downstream applications.

Parametric attributes such as presence of side roads, number of lanes or distance to intersection may be easily annotated by humans given sensor inputs, in particular, requiring less effort than pixel-level semantic annotations. However, besides parametric annotations<sup>1</sup> in the top-view, previous

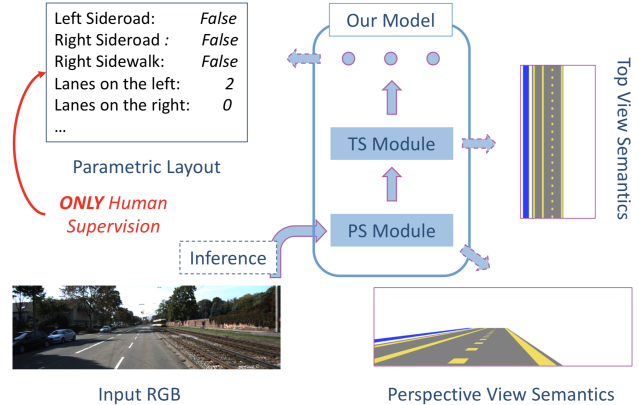


Figure 1. We propose an end-to-end model that requires only the parametric layout annotations during training. Our model is able to output (1) pixel-level semantics in perspective view, (2) pixel-level semantics in top-view and (3) top-view layout attribute predictions. Note that our first two representations are occlusion-reasoned (see the predicted semantics on regions occluded by cars) and are obtained without pixel-level human annotations.

works that estimate parametric top-view layouts also require pixel-level supervision in perspective images [39, 21]. This paper seeks to obtain parametric top-view maps, using only the cheaper form of supervision on attributes. As a by-product of our design, we also obtain pixel-level semantics in both the perspective and top-views.

While relying on cheap supervision only is undoubtedly a goal worth pursuing, removing the dense perspective supervision makes the problem harder. This is non-trivial, since there exists a large gap between sparse parametric supervision and dense pixel-level semantic supervision. To bridge the gap, one must figure out the underlying geometry to map the parametric supervision to top-view and get the correct semantics, even in occluded regions.

We address this challenge through two key insights. First, rather than directly regressing the parametric bird-eye-view(BEV)<sup>2</sup> layout from RGB image space, we introduce two intermediate modules — Perspective Semantics (PS) module and Top-view Semantics (TS) module — to predict

able in our paper.

<sup>2</sup>BEV and top-view are interchangeable in our paper.

intermediate occlusion-reasoned per-pixel perspective and top-view layouts. Second, the parametric annotations can be converted to occlusion-reasoned per-pixel annotations in both the top-view and perspective view, by exploiting a simple renderer and thereafter a geometric transformation, respectively.

Further, our approach allows meaningful deep supervision [16, 17] of intermediate modules without additional annotation costs. Our deep supervision, on the one hand, is beneficial in terms of obtaining meaningful occlusion-reasoned pixel-level semantics in both perspective and top-view without per-pixel human annotations. On the other hand, it also improves our final parametric layout predictions in BEV. Together, these two insights drive the Perspective Semantics (PS) module and Top-view Semantics (TS) module to introduce inductive biases on the type of reasoning the network should perform, thereby facilitating complex tasks such as occlusion reasoning, geometric transformation and semantic abstraction that corresponds to the parametric supervision (See Fig. 1).

We validate the concept of the intermediate modules on KITTI [7] and NuScenes [23], and obtain the state-of-the-art (SOTA) accuracy. We demonstrate that our method even outperforms previous methods that rely on perspective-view dense supervision for semantic segmentation. This verifies our intuitions on the benefits of the deeply supervised modules for perspective and top-view semantics.

To summarize, our key contributions are:

- An end-to-end model for occlusion-reasoned perspective and top-view parametric layout in complex scenes.
- Intermediate module design that incorporates inductive biases to learn occlusion-reasoning, geometric transformation and semantic abstraction.
- Deep supervision with cheap parametric annotations, rather than expensive per-pixel labeling.
- State-of-the-art results on publicly available datasets.

## 2. Related Work

3D scene understanding on outdoor scenes is an important yet challenging task in computer vision. Applications such as robot navigation [11], autonomous driving [6, 15], augmented reality [1] or real estate [22, 32] always require comprehensive understanding on given scenes.

**Road Scene Understanding:** Scene understanding for outdoor scenarios is very challenging mainly due to the lack of strong priors. To this end, non-parametric approaches have been proposed [10, 33, 34], where layered representations are utilized to reason about the geometry as well as semantics in occluded areas. Other typical non-parametric

representations in perspective view are joint pixel-level semantics and depth [19], pixel-level semantics and geometric labels [9]. In contrast, parametric approaches provide abstract understanding, such as road scene attributes [29, 6] and graph-based representation [15]. Perhaps [39, 21] are the most recent works that are able to handle complex road layout, e.g. multiple lanes and different types of intersections. Our work follows the parametric representation proposed in these methods. Unlike [39, 21] that request additional information, e.g. models [13] pre-trained with dataset-specific per-pixel semantics, depth and 3D objects [7], to map semantics to top-view as pre-processing, our model is end-to-end trainable that directly takes RGB as input. More importantly, we exploit deep supervision [16, 17] by introducing meaningful intermediate modules (PS and TS), with which we are able to obtain occlusion-reasoned pixel-level semantics in both perspective and top-view without per-pixel human annotations. It is also beneficial in terms of improving final parametric layout predictions. Please also note that although we focus only on single images, our model can be easily extend to video-version by introducing spatio-temporal graphical model [20, 39], LSTM [4, 31] or FTM [40, 41, 35]

**Scene Understanding in Top-view:** Top-view representations can be more beneficial when occlusion relationships are desired, e.g., two objects cannot occupy the same position in top-view while they can potentially occlude each other in perspective view. Such intuition is widely exploited in 3D object localization literature [37] where camera to top-view projection is fulfilled with the help of depth estimation and 2D detection in perspective view. Although [26] proposes an end-to-end trainable model that explicitly exploits the perspective to top-view projection to perform 3D localization task, the performance of this method is not comparable to [37] due to the lack of explicit depth-aware re-projection. As for general scene understanding, the initial steps are taken in [28, 30]. However, due to the lack of ground truth, no quantitative evaluation is performed in [28]. More recent work [25, 24] extends [26] and predicts top-view semantic map from single monocular image or multiple streams of images. In contrast to non-parametric approaches [25, 24] that require expensive per-pixel supervision in top-view and focus on predicting semantics on visible regions, our method aims to predict parametric layouts in BEV and also provides occlusion-aware non-parametric representations in both BEV and perspective view as by-products. All these meaningful representations are obtained without per-pixel human annotations but relying on cheap parametric annotations.

## 3. Our Framework

Our model consists of three modules. (1) Perspective Semantics (PS) module inputs the RGB image and outputs the Occlusion-reasoned pixel-level Semantics in Perspective

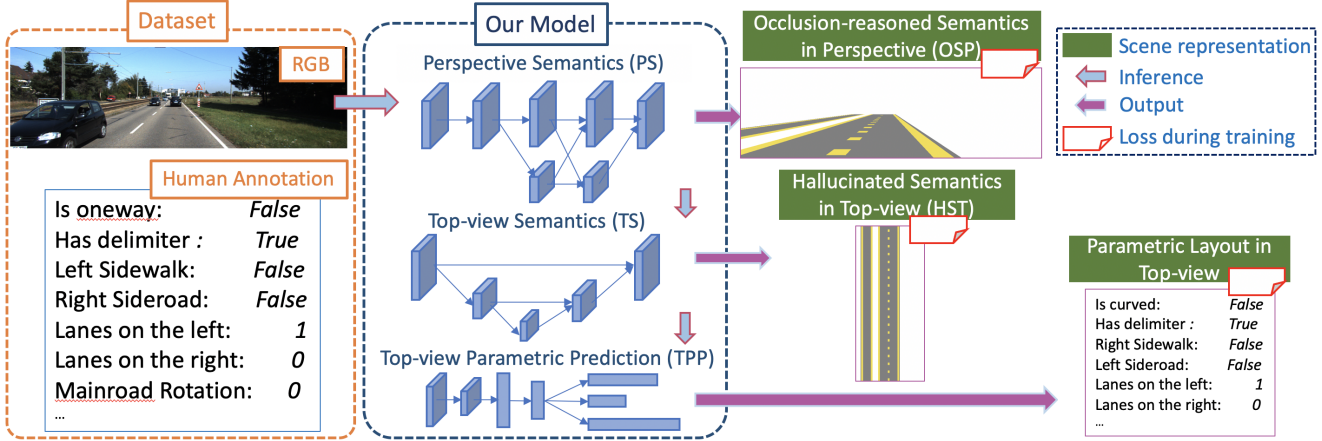


Figure 2. **Overview of our proposed framework:** Taking a single RGB as input, our model predicts (1) occlusion-reasoned semantics in perspective view, (2) hallucinated semantics in top-view and (3) parametric layout predictions in top-view, with only *attribute-level* annotations in top-view. This is achieved with multiple intermediate modules and deeply supervised training.

view (OSP). (2) Top-view Semantics (TS) module projects OSP into top-view and learns to hallucinate/complete pixel-level top-view semantics on out-of-view as well as noisy regions, which we refer to as Hallucinated Semantics in Top-view (HST). (3) Top-view Parametric Prediction (TPP) module takes the HST and predicts road layout related attributes in top-view. Fig. 2 gives an overview of the proposed method. Note that we borrow existing network architectures [36, 27, 39], as our main contributions instead lie in effectively exploiting weak supervision with cheap parametric-level human annotations. We detail each module in Sec. 3.1 and our training with deep supervision in Sec. 3.2.

### 3.1. Full Model

Let us first assume that we have collected a data set  $\mathcal{D} = \{I, x^p, x, \Theta\}_{i=1}^N$  of  $N$  samples. Specifically,  $I \in \mathbb{R}^{H \times W \times 3}$  is the RGB perspective image, with height  $H$  and width  $W$ .  $x^p \in \mathbb{R}^{H \times W \times (C+1)}$  denotes semantic segmentation map in perspective view, with  $(C+1)$  semantic categories (“road”, “sidewalk”, “lane boundaries”, “crosswalks” and “foreground”).  $C = 4$  denotes the number of background categories. We further denote semantic top-views as  $x \in \mathbb{R}^{h \times w \times (C+1)}$ , with spatial dimensions  $h \times w$ , containing the same  $C+1$  semantic categories. Finally, for each data sample, we denote its corresponding scene attributes as  $\Theta$ .

Our full model is defined as:

$$\Theta = f^{\text{full}}(I) = (f^{\text{tpp}} \circ f^{\text{ts}} \circ f^{\text{ps}})(I), \quad (1)$$

where  $\circ$  defines a function composition.  $f^{\text{ps}}$ ,  $f^{\text{ts}}$  and  $f^{\text{tpp}}$  correspond to our three modules PS, TS, and TPP.

#### 3.1.1 Perspective Semantics Module

The PS module predicts per-pixel occlusion-reasoned semantics in the perspective view (OSP). Note that compared to

traditional semantic segmentation models (e.g. [36, 2]) that predict semantics on visible pixels only, our module focuses on predicting both visible and occluded background classes (See Fig. 3(d)). Such occlusion reasoning is also demonstrated in Fig. 3(b) and (c). As shown, we aim to predict road semantics in the top-view despite that they are occluded, e.g. by cars and buildings, in the perspective view.

Compared to conventional semantic segmentation problem, ours is more challenging in terms of both data and model training. As for data, the semantic ground-truth on occluded regions can be ambiguous, hence difficult and time-consuming to annotate accurately in pixel-level. For instance, it takes more than 20 minutes to annotate only the visible regions on KITTI images while in comparison, parametric annotation in BEV takes about 20s for an image [38]. We refer the readers to Sec. 4 and supplementary for annotation details. As for model training, our module predicts semantics in invisible/occluded regions, which again leads to ambiguity. For instance, regions occluded by a foreground instance, e.g. building, can be either another building or road. This requires the module to learn to predict semantics with contextual cues rather than fully relying on visible information.

Assuming that such desired ground-truths,  $x^p$ , are available in our dataset, we then follow the structure of [36], or HRNetV2-W18, as our semantic segmentation backbone as it achieves very good trade-offs between accuracy and efficiency. Formally, given an  $I \in \mathbb{R}^{H \times W \times 3}$ , the PS module would output a  $x^p \in \mathbb{R}^{H \times W \times (C+1)}$ , which denotes the probability of each pixel belongs to specific category.

We define the PS module as:

$$x^p = f^{\text{ps}}(I). \quad (2)$$

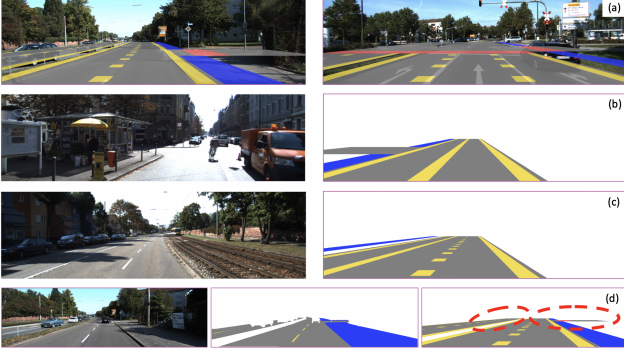


Figure 3. We overlay output and input of PS module in the (a). Examples of inputs (left) and target outputs (right) of PS module are provided in (b) and (c). PS module aims to predict both visible and occluded background classes. (d) demonstrates the input image, semantics of visible regions and our target output from left to right. And we highlight the occluded regions in red.

### 3.1.2 Top-view Semantics Module

Our second module, i.e. the Top-view Semantics module, takes as input the OSP and learns to explicitly project the semantics in perspective view to top-view. Formally, this module takes the input  $x^p \in \mathbb{R}^{H \times W \times (C+1)}$  and outputs  $x \in \mathbb{R}^{h \times w \times (C+1)}$ . Given camera parameters, it seems that the projection is trivial if one has the depth estimation available, say, via a depth network. However, there are several problems in this simple solution. First of all, pixel-wise dense depth estimation with single image as input can be inaccurate. With [19] or without [8, 5] ground-truth supervision, depth accuracy can be unsatisfactory on far away regions and boundaries. Furthermore, standard single image depth network typically do not reason depth in occluded regions, which is nevertheless required for our occlusion-aware projection. In addition, resolution is low for distant regions and thus may lead to sparser/noisier semantics in top-view. Lastly, top-view semantics on close-by regions can be incomplete due to limited field of view.

In view of these challenges, we first make use of the prior that the road forms nearly a plane, which facilitates the projection without requiring depth estimation. We term this step a transformation module. Second, we introduce a hallucination module to address the sparser/noisy semantics and incomplete predictions on far-away and close-by regions in top-view.

**Transformation module.** We assume known camera intrinsics and extrinsics w.r.t. to the ground plane; this is a mild assumption since they could be obtained a prior via calibration [12] in advance. As such, it is well-known [12] that one can back project each pixel in the perspective view to the BEV view and vice versa.

**Hallucination module.** After the transformation module that maps the OSP to top-view, the hallucination module

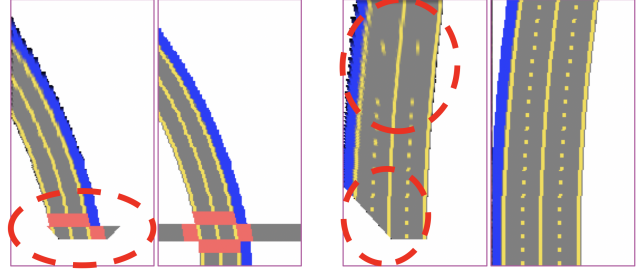


Figure 4. Two sets of examples for input and output of hallucination module. Our module aims to recover the far away sparse semantics (right) and hallucinate close-by areas with limited view (left).

then learns to predict the unseen far away regions as well as recover the noisy semantics with contextual information in top-view. We borrow the structure from [27] and utilize a shallow version, e.g. 5-layer encoder and decoder, as our hallucination module. Note that our input and output of hallucination module are both of the size  $h \times w \times (C+1)$ . Fig. 4 visualizes two sets of inputs and outputs of this module. Compared to inputs that generated with ground-truth OSP, the target HST improves at far away (right) regions as well as close-by area where predictions are limited/noisy (left).

In summary, we define the TS module as:

$$x = f^{\text{ts}}(x^p) = (f^{\text{halln}} \circ f^{\text{trans}})(x^p), \quad (3)$$

where  $f^{\text{halln}}$  and  $f^{\text{trans}}$  are the hallucination and transformation module, respectively.

### 3.1.3 Top-view Parametric Prediction Module

Given the Hallucinated Semantics in Top-view (HST), our next step is to predict the layout attributes. As aforementioned, we follow the attribute definition in [39, 21]. In brief, we introduce the Top-view Parametric Prediction (TPP) module that maps the HST  $x$  into the scene model parameters  $\Theta$ . Our  $\Theta$  consists of three groups— $\Theta_b$  for 14 binary,  $\Theta_m$  for 2 multi-class and  $\Theta_c$  for 10 continuous attributes of scene model, respectively. Binary attributes consists of information like whether the road is one-way or not. Number of lanes on the left hand-side of the ego car is an example of the multi-class attribute and distance to right side-road can be one of the continuous attributes. We refer readers to supplementary materials for more details on scene attribute definition.

Our TPP module is defined as:

$$\Theta = f^{tpp}(x) = (f \circ g)(x), \quad (4)$$

where  $f$  and  $g$  are respectively multi-layer perceptron (MLP) and convolutional neural networks. Specifically,  $f$  is implemented as a multi-task network with three separate predictions  $\eta_b$ ,  $\eta_m$  and  $\eta_c$  for each of the parameter groups  $\Theta_b$ ,  $\Theta_m$

and  $\Theta_c$  of the scene model. And  $g$  is introduced for feature extraction. Note that similar to [39], this module is also able to exploit rich simulated data during training. We leave this extension to future work.

### 3.2. Model Training

Following our above description of intermediate modules assuming supervision available, we describe in this section the generation of such supervision with only annotations for parametric layout  $\Theta$ , as well as deep supervision training. Instead of training the full model in an end-to-end manner from scratch in the very beginning, we propose a multi-stage training protocol. After pretraining all three modules, we then relax all modules and learn the full model in an end-to-end manner. In practice, end-to-end training provides a 1% performance improvement in our experiments.

Our full loss function  $\mathcal{L}$  is defined as:

$$\mathcal{L} = \lambda \times \mathcal{L}^{\text{tpp}} + \gamma \times \mathcal{L}^{\text{ts}} + \beta \times \mathcal{L}^{\text{ps}} \quad (5)$$

where  $\lambda$ ,  $\gamma$  and  $\beta$  are the weights for each module.

**Loss Functions on Top-view Parametric Prediction Module:** Since  $\Theta$  and  $I$  are already available,

$$\mathcal{L}^{\text{tpp}} = \sum_{i=1}^N \text{BCE}(\Theta_{b,i}, \eta_{b,i}) + \text{CE}(\Theta_{m,i}, \eta_{m,i}) + \ell_1(\Theta_{c,i}, \eta_{c,i}), \quad (6)$$

where (B)CE is the (binary) cross-entropy loss and  $\ell_1$  denotes L1 loss.  $\{\Theta, \eta\}_{\cdot, i}$  denotes the  $i$ -th sample in the data set. For regression, we discretize continuous variables into 100 bins by convolving a dirac delta function centered at  $\Theta_c$  with a Gaussian of fixed variance. Such multi-modal predictions allow potential application of our model output with subsequent probabilistic graphical models.

#### 3.2.1 Top-view Semantics Module

Unlike the straightforward design in parametric space, our second module requires per-pixel supervision in top-view. To this end, we propose to exploit a rendering function that generates pixel-wise semantics from parametric annotations. Specifically, for each  $\Theta$ , we will render a map  $x$ . Some examples of our paired  $\{x, \Theta\}$  can be found in Fig. 5, which shows that our rendered  $x^p$  accurately reflects the layout of the road in top-view. Since we only need on parametric abstractions, our renderer can be implemented using simple Python code, rather than the complex machinery of image renderers. We refer the readers to supplementary materials for more details on our renderer.

**Loss Functions on Top-view Semantics Module:** The loss function for TS module is defined as:

$$\mathcal{L}^{\text{ts}} = \sum_{i=1}^N \text{CE}(x_i, \hat{x}_i) \quad (7)$$



Figure 5. Examples of rendered ground-truth for TS module. From left to right: RGB, parametric human annotations and rendered pixel-level semantics in top-view.

where  $\hat{x}_i$  and  $x_i$  denotes the predictions and the rendered ground-truth of the top-view semantics of  $i$ -th sample in  $\mathcal{D}$ .

#### 3.2.2 Perspective Semantics Module

Obtaining the top-view semantics  $x$ , we can project [12] it to perspective view with camera parameters as well as plane assumption. Fig. 3(a) demonstrates the effectiveness of our mapping. Our back projection can indeed recover the occluded regions and aligns the semantics well with respect to input image in perspective view.

**Loss Functions on Perspective Semantics Module:** Similarly, we introduce the loss function for PS module as:

$$\mathcal{L}^{\text{ps}} = \sum_{i=1}^N \text{CE}(x_i^p, \hat{x}_i^p) \quad (8)$$

where  $\hat{x}_i^p$  and  $x_i^p$  denotes our predictions and the back-projected ground-truth of the perspective semantics of  $i$ -th sample in  $\mathcal{D}$ .

## 4. Experiments

**Datasets and Model Details:** We validate our ideas on KITTI [7] and NuScenes [23], utilizing the annotation and data split in [21]<sup>3</sup>.  $h$  and  $w$  are set to 256 and 128, presenting a  $60\text{m} \times 30\text{m}$  space in real world. Camera parameters are available in the original datasets [7, 23] through calibration. Weights  $(\lambda, \gamma, \beta)$  are set experimentally on validation set.

**Parametric annotations:** We summarize the annotation time for each type of supervision in Tab. 2. Unlike non-parametric annotations such as pixel-level semantics that require several dozens of minutes per frame, our parametric annotations require less than a minute per frame. Moreover, this time is heavily amortized across a video sequence to just around 20 seconds on the KITTI dataset, since parametric attributes change predictably across consecutive frames. Binary and multiclass attributes (such as presence of side-road, or number of lanes) change less frequently and their

<sup>3</sup>It includes around 17000 annotations for KITTI and about 1200 annotations for NuScenes in terms of scene layout annotation.

Method	Supervision Required					KITTI [7]			
	Parametric	Depth	Semantics	Simulated	Video+Object	Accu.-Bi. $\uparrow$	Accu.-Mc. $\uparrow$	MSE $\downarrow$	F1 $\uparrow$
RGB [29, 13]	✓					.811	.778	.230	.176
RGB [29, 13]+D	✓	✓				.818	.819	.154	.109
BEV [28]	✓	✓	✓			.820	.797	.141	.324
H-BEV+DA [39]	✓	✓	✓	✓		.834	.831	.134	.435
BEV-J-O [21]	✓	✓	✓		✓	.831	.837	.142	.494
Ours	✓					.833	.832	.140	.473

Table 1. Performances on single image based road layout prediction on KITTI. we observe that our method beats *RGB* when having the same model setting. In addition, our results are comparable to other SOTA (*H-BEV+DA* and *BEV-J-O*) but with far less human annotations required.

Time	Binary	Multiclass	Continuous	Total
Random images	24.3	5.1	25.7	55.1
Video frames			20.2	

Table 2. Average annotation time (sec.) on KITTI dataset.

annotations can often be inherited from previous frames. Further, continuous attributes (such as distance to intersection) typically change smoothly across frames, which facilitates annotation. We refer the readers to supplementary materials for more details. Our annotations will be publicly released.

**Evaluation metrics:** Since our output space  $\Theta$  consists of three types of predictions and involves both discrete and continuous variables, we follow the metrics in [39, 21]. Specifically, as for binary variables  $\Theta_b$  and multi-class variables  $\Theta_m$ , the prediction accuracy is defined as  $\text{Accu.-Bi} = \frac{1}{14} \sum_{k=1}^{14} [p_k = \Theta_{bk}]$  and  $\text{Accu.-Mc} = \frac{1}{2} \sum_{k=1}^2 [p_k = \Theta_{mk}]$ . We further report the F1 score on  $\Theta_b$  to have a better idea about the overall performance given the observation that the binary classes are extremely biased. Formally,  $\text{F1} = \frac{1}{14} \sum_{k=1}^{14} 2 \times \frac{p_k \times r_k}{p_k + r_k}$ , where  $p_k$  and  $r_k$  are the precision and recall rate on  $\Theta_{bk}$ . For continuous variables, we report the mean square error (MSE).

Apart from parametric predictions, our model also outputs intermediate representations, e.g. OSP and HST. We further report the IoU as well as the accuracy for these two semantic segmentation tasks. Please note that since we do not have human annotated per-pixel ground-truth for these two tasks, we report our performance by comparing our predictions with rendered semantics  $x$  and  $x^p$  instead.

#### 4.1. Evaluations of Parametric Road Layout

**Baselines:** We choose several appropriate baselines as presented in [39, 21].:

- **RGB (RGB):** A ResNet-101 [14]) backbone is introduces and trained on the manually-annotated ground truth. Note that this setup is the **Only** one that directly comparable to ours as it requires only the parametric annotations as ground-truth.
- **RGB+Depth (RGB+D):** Same as RGB but with the additional task of monocular pixel-wise depth prediction.

In contrast, we do not require dense depth information.

- **BEV (BEV):** BEV uses the output of [28], which is a top-view semantic map. Note that to obtain such map, additional pixel-level semantic annotation and depth supervision are required in perspective space.

We also report the performance of SOTA methods for single image top-view layout prediction, or **H-BEV-DA** and **BEV-J-O** in [39, 21]. Please note that both of them require far more human annotations compared to our method.

**Quantitative results:** Tab. 1 summarizes our main results on KITTI [7]. First of all, if we compare only to method with the same setting, or *RGB*, our method outperforms it with a large margin, which indicates the effectiveness of introducing PS and TS as intermediate modules. Furthermore, compared to *RGB + D* method that introduces depth channel, or even the *BEV* that further requires thousands of human labelled semantic segmentation images in perspective space, our method achieves better results, which is of significance given that our method requires far less human annotations. Note that both **H-BEV-DA** and **BEV-J-O** are based on *BEV* but require even more human annotations. By comparing to **H-BEV-DA** that further exploits additional simulated data and **BEV-J-O** that requires the 3D object information as well as entire video sequence as input, we can see that our method achieves comparable results with far less human annotations.

We further report results on NuScenes [23] in Tab. 3. Our method beats *RGB* significantly. It also outperforms [21, 39] with far less human annotations required.

**Qualitative results:** We demonstrate some qualitative results in Fig. 6. Note that in KITTI test sequences, rather than the road being occluded by cars driving in front, significant occlusions happen between parked cars and road/sidewalk, or between foreground classes, e.g. buildings or trees, and curved road or sideroad. As observed in this figure, our model is able to output satisfactory results on all three representations. We are able to handle complex road layout such as arbitrary number of lanes with heavy occlusions. Again, please note that OSP and HST are obtained without per-pixel

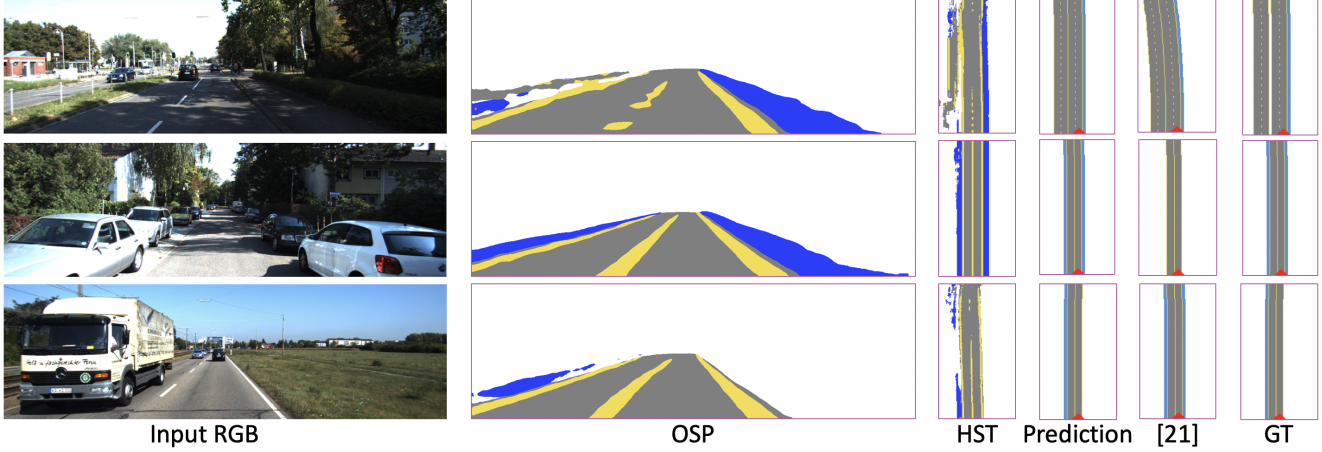


Figure 6. Full predictions of our proposed model. From left to right: input RGB, OSP, HST, image rendered from parametric predictions, results from [21] and image rendered from ground-truth attributes.



Figure 7. Examples on NuScenes dataset. Left:input RGB Right: rendered BEV semantics from our prediction.

human annotations. Our final layout prediction is also better than [21]. We further visualize our final results on NuScenes in Fig. 7. It can be seen that our model is able to handle various road layouts. We refer readers to supplementary material for more qualitative results.

**Occlusion study:** Here, we study performance against increasing number of objects in the scene, indicating increasingly severe occlusions. Since [38, 7] do not provide pixel-level semantic ground-truths on our test sequences, to analyze our ability to handle occlusions, we instead report the average image-level IoU on four classes against number of foreground objects with respect to rendered ground truth  $x$  in Tab. 6, with objects detected by Stereo-RCNN [18]. As one can see, our method outperforms the state-of-the-art consistently, with increasing gap when having more objects.

## 4.2. Ablation Study

To demonstrate the effectiveness of intermediate modules as well as deep supervision, we further conduct experiments on incrementally adding modules.  $RGB$  is the one without any module.  $RGB+PS$  contains the PS module and directly predicts parametric predictions with perspective outputs. Formally,  $RGB+PS$  is formulated as:

$$\Theta = f^{rbgp}(I) = (f^{tpp} \circ f^{ps})(I), \quad (9)$$

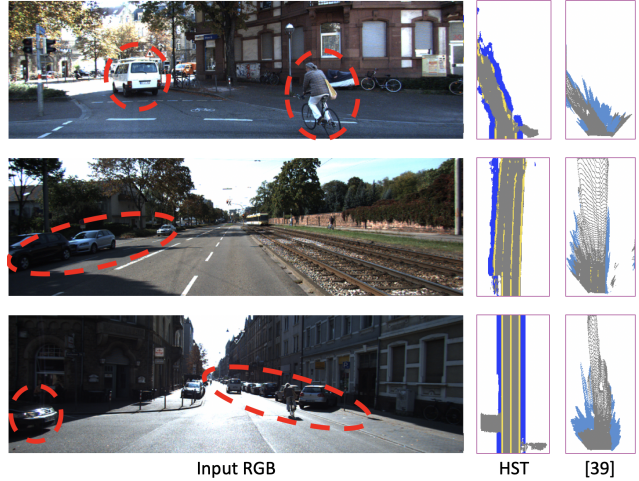


Figure 8. We demonstrate input RGB, predicted HST as well as BEV of [39], which is trained with thousands of pixel-level annotated images and LiDAR images. As can be seen in these examples, our model is able to hallucinate far away regions in a realistic manner, even on curved road, with *NO* pixel-level human annotations.

Similarly,  $RGB+PS+T$  is formulated as:

$$\Theta = f^{rbgpf}(I) = (f^{tpp} \circ f^{trans} \circ f^{ps})(I), \quad (10)$$

We report the quantitative results in Tab. 4. The results show that first of all, comparing the  $RGB$  to  $RGB+PS$ , perspective representation, or the OSP, is beneficial in terms of improving final parametric predictions. Secondly, the performance gap between  $RGB+PS+T$  and  $RGB+PS$  demonstrates the effectiveness of introducing top-view semantics as intermediate representation. Finally, by comparing the full model with  $RGB+PS+T$ , we can tell that the hallucination module is also critical to further boost the final performance.

Method	Accu.-Bi. $\uparrow$	Accu.-Mc. $\uparrow$	MSE $\downarrow$	F1 $\uparrow$
RGB [29, 13]	.850	.503	.084	.109
BEV [39]	.846	.485	.073	.101
H-BEV+DA [39]+GM	.877	.496	.032	.125
BEV-J-O [21]	.858	.543	.027	.128
Ours	.875	.560	.023	.130

Table 3. Results on NuScenes dataset. We observe that our method beats *RGB* significantly when having the same model setting. Meanwhile, it also outperforms *H-BEV+DA* and *BEV-J-O* with far less human annotations required.

Method	Module				KITTI [7]			
	Perspective	Transformation	Hallucination	Parametric	Accu.-Bi. $\uparrow$	Accu.-Mc. $\uparrow$	MSE $\downarrow$	F1 $\uparrow$
RGB [29]				✓	.811	.778	.230	.176
RGB+PS	✓			✓	.822	.827	.159	.425
RGB+PS+T	✓	✓		✓	.826	.829	.144	.441
Ours	✓	✓	✓	✓	.833	.832	.140	.473

Table 4. Ablation study on single image based road layout prediction on KITTI. Note that all these methods share the same amount of human annotations. We can see that our introduced PS and TS modules, on the one hand, provide meaningful intermediate representations at no additional costs. On the other hand, they also prove to be beneficial individually for the final parametric prediction task.

Data	Representation		KITTI [7]											
	OSP	HST	Road		Land Boundary		Sidewalk		Crosswalk		Foreground		Average	
			Accu.	IoU	Accu.	IoU	Accu.	IoU	Accu.	IoU	Accu.	IoU	Accu.	IoU
RGB+PS	✓		.689	.563	.365	.214	.226	.126	.010	.007	.954	.878	.449	.358
Ours	✓		.700	.605	.403	.272	.255	.147	.042	.033	.962	.883	.472	.388
		✓	.605	.461	.272	.197	.167	.102	.038	.032	.868	.651	.390	.289

Table 5. Intermediate results on KITTI. We report both IoU and accuracy for each semantic category. Compared to *RGB+PS*, our method achieves better performance in terms of *OSP* with the help of end-to-end training. Our method further provides meaningful *HST* results.

Obj.	0	1	2	3	4	5	6	7	8	Avg.
[39]	.67	.78	.67	.64	.61	.45	.48	.37	.35	.45
Ours	.78	.81	.72	.69	.67	.48	.50	.40	.35	.50
Considering Road Class Only										
[39]	.85	.74	.85	.79	.67	.63	.59	.57	.37	.63
Ours	.86	.91	.86	.83	.70	.70	.61	.61	.50	.70

Table 6. Average per-image IoU w.r.t. number of road participants.

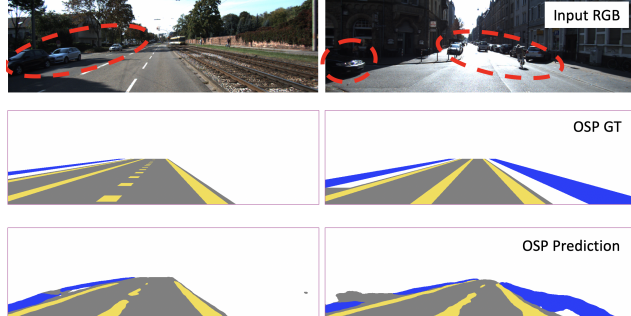


Figure 9. Input image, generated ground-truth pixel-level semantics and predicted semantics from top to bottom row. Our model is able to predict the semantics quite well despite occlusions.

### 4.3. Evaluations of Intermediate Representations

Apart from requiring less annotation while maintaining comparable performance, another advantage of the proposed method is being able to provide meaningful pixel-level intermediate representations, OSP and HST, as by-products. To demonstrate that these intermediate representations are indeed semantically useful for downstream tasks, we study their IoU as well as accuracy score, as an indication for their performance. Please note that compared to existing work that requires dense and time-consuming pixel-wise human annotation, ours only requires cheap parametric human anno-

tations and produces pixel-level occlusion-reasoned semantic segmentation in perspective and top-view.

As shown in Tab. 5, our method is able to provide multiple meaningful intermediate representations. Also, our deep supervision proves to be beneficial in an end-to-end manner, which can be observed from the performance gap on OSP between *RGB+PS* and our full model. In addition, our model also achieves reasonably good performance on HST. As a reference, [25], which aims to predict pixel-level semantics of visible regions in top-view with perspective images as input, reports about 63.0% IoU for drivable category on two different datasets. However, please note that [25] requires pixel-level dense annotations in top-view during training and the predictions are not occlusion-reasoned. We further visualize quantitative results in Fig. 8 and Fig. 9. As can be seen, our method obtain high quality semantics in both perspective and top-view despite occlusions.

## 5. Conclusion

In this paper, we propose a novel end-to-end model that inputs the RGB perspective image and outputs multi-aspect representations for road layout, including top-view parametric predictions, OSP and HST. Specifically, we introduce two intermediate modules, PS and TS, to learn inductive biases in occlusion-reasoning, geometric transformation and semantic abstraction. More importantly, we exploit deep supervision during training with very cheap parametric annotations, without any per-pixel human supervision. We demonstrate the effectiveness of our proposed method on publicly available datasets and demonstrate that we can achieve state-of-the-art performance with far less human annotations. We also conduct detailed experiments to demonstrate the effectiveness and usefulness of intermediate modules.

## References

[1] Iro Armeni, Ozan Sener, Amir R. Zamir, Helen Jiang, Ioannis Brilakis, Martin Fischer, and Silvio Savarese. 3D Semantic Parsing of Large-Scale Indoor Spaces. 2016. 2

[2] Liang-Chieh Chen, George Papandreou, Iasonas Kokkinos, Kevin Murphy, and Alan L Yuille. Semantic image segmentation with deep convolutional nets and fully connected crfs. *arXiv preprint arXiv:1412.7062*, 2014. 3

[3] Vikas Dhiman, Quoc-Huy Tran, Jason J. Corso, and Manmohan Chandraker. A Continuous Occlusion Model for Road Scene Understanding. 2016. 1

[4] Christoph Feichtenhofer, Axel Pinz, and Richard P Wildes. Spatiotemporal multiplier networks for video action recognition. In *Proceedings of the IEEE conference on computer vision and pattern recognition*, pages 4768–4777, 2017. 2

[5] Ravi Garg, Vijay Kumar Bg, Gustavo Carneiro, and Ian Reid. Unsupervised cnn for single view depth estimation: Geometry to the rescue. In *European conference on computer vision*, pages 740–756. Springer, 2016. 4

[6] Andreas Geiger, Martin Lauer, Christian Wojek, Christoph Stiller, and Raquel Urtasun. 3D Traffic Scene Understanding from Movable Platforms. 2014. 1, 2

[7] Andreas Geiger, Philip Lenz, Christoph Stiller, and Raquel Urtasun. Vision meets Robotics: The KITTI Dataset. *International Journal of Robotics Research (IJRR)*, 2013. 2, 5, 6, 7, 8

[8] Clément Godard, Oisin Mac Aodha, and Gabriel J Brostow. Unsupervised monocular depth estimation with left-right consistency. In *Proceedings of the IEEE Conference on Computer Vision and Pattern Recognition*, pages 270–279, 2017. 4

[9] Stephen Gould, Richard Fulton, and Daphne Koller. Decomposing a scene into geometric and semantically consistent regions. In *2009 IEEE 12th international conference on computer vision*, pages 1–8. IEEE. 2

[10] Ruiqi Guo and Derek Hoiem. Beyond the line of sight: labeling the underlying surfaces. 2012. 2

[11] Saurabh Gupta, James Davidson, Sergey Levine, Rahul Sukthankar, and Jitendra Malik. Cognitive Mapping and Planning for Visual Navigation. 2017. 1, 2

[12] Richard Hartley and Andrew Zisserman. *Multiple view geometry in computer vision*. Cambridge university press, 2003. 4, 5

[13] Kaiming He, Xiangyu Zhang, Shaoqing Ren, and Jian Sun. Deep residual learning for image recognition. In *Proceedings of the IEEE conference on computer vision and pattern recognition*, pages 770–778, 2016. 2, 6, 8

[14] Kaiming He, Xiangyu Zhang, Shaoqing Ren, and Jian Sun. Deep Residual Learning for Image Recognition. 2016. 6

[15] Lars Kunze, Tom Bruls, Tarlan Suleymanov, and Paul Newman. Reading between the Lanes: Road Layout Reconstruction from Partially Segmented Scenes. In *International Conference on Intelligent Transportation Systems (ITSC)*, 2018. 2

[16] Chen-Yu Lee, Saining Xie, Patrick Gallagher, Zhengyou Zhang, and Zhuowen Tu. Deeply-Supervised Nets. In *Proceedings of the Eighteenth International Conference on Artificial Intelligence and Statistics*, 2015. 2

[17] Chi Li, M. Zeeshan Zia, Quoc-Huy Tran, Xiang Yu, Gregory D. Hager, and Manmohan Chandraker. Deep supervision with shape concepts for occlusion-aware 3d object parsing. In *IEEE Computer Society Conference on Computer Vision and Pattern Recognition*, 2017. 2

[18] Peiliang Li, Xiaozhi Chen, and Shaojie Shen. Stereo r-cnn based 3d object detection for autonomous driving. In *Proceedings of the IEEE Conference on Computer Vision and Pattern Recognition*, pages 7644–7652, 2019. 7

[19] Beyang Liu, Stephen Gould, and Daphne Koller. Single image depth estimation from predicted semantic labels. In *2010 IEEE Computer Society Conference on Computer Vision and Pattern Recognition*, pages 1253–1260. IEEE, 2010. 2, 4

[20] Buyu Liu and Xuming He. Multiclass semantic video segmentation with object-level active inference. In *Proceedings of the IEEE conference on computer vision and pattern recognition*, pages 4286–4294, 2015. 2

[21] Buyu Liu, Bingbing Zhuang, Samuel Schulter, Pan Ji, and Manmohan Chandraker. Understanding road layout from videos as a whole. In *Proceedings of the IEEE/CVF Conference on Computer Vision and Pattern Recognition (CVPR)*, June 2020. 1, 2, 4, 5, 6, 7, 8

[22] Chenxi Liu, Alexander G. Schwing, Kaustav Kundu, Raquel Urtasun, and Sanja Fidler. Rent3D: Floor-Plan Priors for Monocular Layout Estimation. 2015. 2

[23] NuTonomy. The NuScenes data set. <https://www.nuscenes.org>, 2018. 2, 5, 6

[24] Jonah Philion and Sanja Fidler. Lift, splat, shoot: Encoding images from arbitrary camera rigs by implicitly unprojecting to 3d. *arXiv preprint arXiv:2008.05711*, 2020. 2

[25] Thomas Roddick and Roberto Cipolla. Predicting semantic map representations from images using pyramid occupancy networks. In *Proceedings of the IEEE/CVF Conference on Computer Vision and Pattern Recognition*, pages 11138–11147, 2020. 1, 2, 8

[26] Thomas Roddick, Alex Kendall, and Roberto Cipolla. Orthographic feature transform for monocular 3d object detection. *arXiv preprint arXiv:1811.08188*, 2018. 2

[27] Olaf Ronneberger, Philipp Fischer, and Thomas Brox. U-net: Convolutional networks for biomedical image segmentation. In *International Conference on Medical image computing and computer-assisted intervention*, pages 234–241. Springer, 2015. 3, 4

[28] Samuel Schulter, Menghua Zhai, Nathan Jacobs, and Manmohan Chandraker. Learning to Look around Objects for Top-View Representations of Outdoor Scenes. 2018. 2, 6

[29] Ari Seff and Jianxiong Xiao. Learning from Maps: Visual Common Sense for Autonomous Driving. *arXiv:1611.08583*, 2016. 2, 6, 8

[30] Sunando Sengupta, Paul Sturgess, Lubor Ladický, and Philip H. S. Torr. Automatic Dense Visual Semantic Mapping from Street-Level Imagery. 2012. 2

[31] Karen Simonyan and Andrew Zisserman. Two-stream convolutional networks for action recognition in videos. In *Advances in neural information processing systems*, pages 568–576, 2014. 2

[32] Shuran Song, Andy Zeng, Angel X. Chang, Manolis Savva, Silvio Savarese, and Thomas Funkhouser. Im2Pano3D: Extrapolating 360 Structure and Semantics Beyond the Field of View. 2018. [2](#)

[33] Joseph Tighe, Marc Niethammer, and Svetlana Lazebnik. Scene Parsing with Object Instances and Occlusion Ordering. June 2014. [2](#)

[34] Shubham Tulsiani, Richard Tucker, and Noah Snavely. Layer-structured 3D Scene Inference via View Synthesis. 2018. [2](#)

[35] Tuan-Hung Vu, Wongun Choi, Samuel Schulter, and Manmohan Chandraker. Memory warps for learning long-term online video representations. *arXiv preprint arXiv:1803.10861*, 2018. [2](#)

[36] Jingdong Wang, Ke Sun, Tianheng Cheng, Borui Jiang, Chaorui Deng, Yang Zhao, Dong Liu, Yadong Mu, Mingkui Tan, Xinggang Wang, Wenyu Liu, and Bin Xiao. Deep high-resolution representation learning for visual recognition, 2020. [3](#)

[37] Yan Wang, Wei-Lun Chao, Divyansh Garg, Bharath Hariharan, Mark Campbell, and Kilian Q Weinberger. Pseudo-lidar from visual depth estimation: Bridging the gap in 3d object detection for autonomous driving. In *Proceedings of the IEEE Conference on Computer Vision and Pattern Recognition*, pages 8445–8453, 2019. [2](#)

[38] Ziyan Wang, Buyu Liu, Samuel Schulter, and Manmohan Chandraker. A dataset for high-level 3d scene understanding of complex road scenes in the top-view. In *The IEEE Conference on Computer Vision and Pattern Recognition (CVPR) Workshop*, June 2019. [3, 7](#)

[39] Ziyan Wang, Buyu Liu, Samuel Schulter, and Manmohan Chandraker. A parametric top-view representation of complex road scenes. In *The IEEE Conference on Computer Vision and Pattern Recognition (CVPR)*, June 2019. [1, 2, 3, 4, 5, 6, 7, 8](#)

[40] Xizhou Zhu, Yujie Wang, Jifeng Dai, Lu Yuan, and Yichen Wei. Flow-guided feature aggregation for video object detection. In *Proceedings of the IEEE International Conference on Computer Vision*, pages 408–417, 2017. [2](#)

[41] Xizhou Zhu, Yuwen Xiong, Jifeng Dai, Lu Yuan, and Yichen Wei. Deep feature flow for video recognition. In *Proceedings of the IEEE Conference on Computer Vision and Pattern Recognition*, pages 2349–2358, 2017. [2](#)